THE RELATIONSHIP BETWEEN BLACK HOLE MASS AND VELOCITY DISPERSION IN SEYFERT 1 GALAXIES

Charles H. Nelson[1]

Physics and Astronomy Department, Drake University, 2507 University Avenue, Des Moines, IA 50311; charles.nelson@drake.edu

Richard F. Green[1,2]

National Optical Astronomy Observatory, P.O. Box 26732, Tucson, AZ 85726

Gary Bower[1]

Space Telescope Science Institute, 3700 San Martin Drive, Baltimore, MD 21218

Karl Gebhardt

Department of Astronomy, University of Texas, Austin, TX 78712

and

Donna Weistrop

Physics Department, University of Nevada at Las Vegas, Box 4002, 4505 Maryland Parkway, Las Vegas, NV 89154

ABSTRACT

Black hole masses in active galactic nuclei are difficult to measure using conventional dynamical methods but can be determined using the technique of reverberation mapping. However, it is important to verify that the results of these different methods are equivalent. This can be done indirectly, using scaling relations between the black hole and the host galaxy spheroid. For this purpose, we have obtained new measurements of the bulge stellar velocity dispersion, σ_*, in Seyfert 1 galaxies. These are used in conjunction with the M_{BH}-σ_* relation to validate nuclear black hole masses, M_{BH}, in active galaxies determined through reverberation mapping. We find that Seyfert galaxies follow the same M_{BH}-σ_* relation as nonactive galaxies, indicating that reverberation mapping measurements of M_{BH} are consistent with those obtained using other methods. We also reconsider the relationship between bulge absolute magnitude, M_{bul}, and black hole mass. We find that Seyfert galaxies are offset from nonactive galaxies, but that the deviation can be entirely understood as a difference in bulge luminosity, not black hole mass; Seyfert galaxy hosts are brighter than normal galaxies for a given value of their velocity dispersion, perhaps as a result of younger stellar populations.

Subject headings: black hole physics — galaxies: kinematics and dynamics — galaxies: nuclei — galaxies: Seyfert — quasars: general

1. INTRODUCTION

An observational problem in research on active galactic nuclei (AGNs) is determining the masses of the central black holes. Application of stellar dynamical and gasdynamical techniques, commonly used for normal galaxies (e.g., Bower et al. 1998; Gebhardt et al. 2003), is difficult or impossible in type 1 AGNs because of the bright nucleus. A potential solution is the technique known as reverberation mapping (Blandford & McKee 1982; Netzer & Peterson 1997), which has been used to estimate black hole masses for ~30 Seyfert galaxies and quasars (Wandel et al. 1999; Kaspi et al. 2000). Reverberation mapping allows the radius of the broad-line region (BLR), R_{BLR}, to be determined by attributing the time lag between variations in the continuum and line emission to light travel time effects. Assuming that the velocity width, W, of the permitted emission lines is due to Keplerian motion in the black hole potential, the mass can estimated by $M_{BH} \sim W^2 R_{BLR}/G$, where G is the gravitational constant. Thus, this method may provide an opportunity to study the role of the nuclear gravitational potential in large numbers of AGNs. However, it has not yet been demonstrated that reverberation mapping yields M_{BH} values that are consistent with those obtained from analyses of the stellar dynamics and gasdynamics. Given the difficulty of a direct approach, indirect methods must be used to compare these different techniques. Our purpose in this study is to compare reverberation mapping and stellar dynamical measures of black hole mass using scaling relations between the black hole and the host galaxy bulge.

The correlation between black hole mass and bulge absolute magnitude, M_{bul} (Kormendy 1993; Kormendy & Richstone 1995), can be used to compare the results of these different approaches. However, comparisons of the M_{BH}-M_{bul} relation in active and normal galaxies have produced conflicting results. Two early studies (Ho 1999; Wandel 1999) reported that the reverberation mapping masses for AGNs were smaller than the stellar dynamical masses in normal galaxies of the same bulge luminosity. This called into question the validity of the reverberation mapping masses, suggesting a systematic trend to underestimate M_{BH} by a factor of ~5 (Ho 1999). Alternatively, Wandel (1999) suggested that the masses were accurate and that there were real differences in the black hole masses

of active and nonactive galaxies of equal bulge mass. More recently, Wandel (2002), revising his early assessment, and McLure & Dunlop (2001), using bulge magnitudes determined in most of their sample from *Hubble Space Telescope* (*HST*) images and assuming disklike kinematics for the BLR, find that active galaxies follow the same M_{BH}-M_{bul} relation as normal galaxies.

It is difficult to make a fair assessment of these differing results, since some of these studies have used bulge magnitudes derived from the bulge-to-disk ratio as a function of morphological type formulated by Simien & de Vaucouleurs (1986), while others have applied bulge-disk decomposition techniques to ground-based or *HST* images. Furthermore, bulges of Seyfert galaxies tend to be small: their typical effective radii in all but the nearest objects are a few arcseconds or less. This, combined with the effects of the bright nuclear source in type 1 objects, which are of course candidates for reverberation mapping, makes ground-based estimates of M_{bul} quite tricky.

The relationship between black hole mass and bulge stellar velocity dispersion, σ_* (Ferrarese & Merritt 2000; Gebhardt et al. 2000a), provides an alternative and independent way to compare stellar dynamical and reverberation mapping results. In this relation, which is stronger than the one using M_{bul}, σ_* is measured in apertures extending to distances of a kiloparsec or so from the nucleus (Gebhardt et al. 2000a use apertures extending to the bulge effective radius, r_e, and denote their measurement σ_e). The goal is to standardize the region over which the dispersion is determined and, more importantly, to minimize the influence of the nuclear black hole on the stellar kinematics.

The small number of published σ_* measurements for type 1 AGNs has until recently prevented a statistically significant investigation. Gebhardt et al. (2000b) found no deviation for seven Seyfert 1 galaxies from the M_{BH}-σ_e relation. The same conclusion was reached by Nelson (2000), using FWHM$_{[O\ III]}$ in place of σ_*, on the assumption that the forbidden line kinematics in Seyfert galaxies are predominantly the result of virial motion in the bulge gravitational potential (e.g., Nelson & Whittle 1996). Also, Ferrarese et al. (2001) obtained σ_* measurements for six Seyfert 1 galaxies and find these values to be consistent with expectations from the M_{BH}-σ_* relation.

In this paper we present new measurements of σ_* in 14 Seyfert 1 galaxies to check the M_{BH} values obtained from reverberation mapping for consistency with the M_{BH}-σ_e relation established by stellar dynamical techniques. Observations of the Ca II triplet lines and velocity dispersion measurements using the Fourier correlation quotient (FCQ) are presented in § 2. Bulge magnitude estimates for 11 of these obtained from *HST* archival data are presented in § 3. Notes on individual sample members are presented in § 4. In § 5 we discuss the results in the context of the M_{BH}-σ_* relation and in § 6 we revisit the M_{BH}-M_{bul} relation to try to determine the origin of the discrepancies noted above. Our results are summarized in § 7.

2. SPECTROSCOPIC DATA

2.1. *Observations and Reductions*

Long-slit spectroscopy of 16 Seyfert 1 galaxies and several stellar template stars was obtained on two observing runs (UT 2001 April 10–14 and November 1–4) using the 4 m telescope at Kitt Peak National Observatory. Our sample is composed of Seyfert 1 galaxies included in long-term emission line and continuum monitoring campaigns for which reverberation mapping estimates of M_{BH} have been published (Kaspi et al. 2000; Wandel et al. 1999; Ho 1999). The Ritchey-Chrétien (RC) spectrograph

was used with the LB1A CCD, which has high quantum efficiency in the far-red (~90% at 8500 Å), excellent cosmetics, and no fringing (Dey et al. 2001): an ideal detector for observing the Ca II triplet lines (at 8498.0, 8542.1, and 8662.1 Å). These properties allowed us to use a high-dispersion grating (BL 380, giving 0.46 Å pixel^{-1} in the raw data) and a narrow slit (1″) to achieve high spectral resolution (~1.1 Å or ~40 km s^{-1} FWHM). We used an order-blocking filter (OG570) to prevent contamination by second-order blue light, which will of course be strong in Seyfert 1 galaxy spectra. Exposure times ranged between 3600 s for nearby bright galaxies (e.g., NGC 4051 and NGC 3516) and 10,800 s for fainter objects (e.g., Mrk 110). Standard spectroscopic reductions (bias subtraction, flat field correction, geometric distortion, and wavelength calibration) were carried out using IRAF. Conditions were generally not photometric, so only a relative flux calibration was applied.

The strong telluric emission and absorption features in the far-red present a difficult reduction problem, particularly for the higher redshift galaxies in our sample. For targets with $z \geq 0.016$, where the Ca II triplet and night sky emission lines begin to overlap (except 3C 390.3; see § 4), sky subtraction was accomplished using the "nod-and-shuffle" observation mode developed by Glazebrook & Bland-Hawthorn (2001) and recently implemented at Kitt Peak. Briefly, by repeatedly repositioning the telescope (nodding) and shifting the charge on the detector (shuffling), both the target and the sky are observed at the same spot along the slit and in the same pixels on the detector, permitting excellent sky subtraction. The drawbacks for the nod-and-shuffle technique are a factor of $\sqrt{2}$ increase in the sky noise and extra overhead time for the telescope nods. Although there were difficulties in the implementation of this mode at the time, we were quite pleased with the results and we recommend use of the perfected observing mode where sky subtraction is critical and the signal-to-noise ratio is not of primary concern.

Atmospheric absorption bands begin to be a problem at wavelengths above 8900 Å, again affecting the higher redshift members of the sample. Even if the Ca II triplet lines are not directly affected, correction for these can be important for achieving a good fit to the continuum on the red side. We therefore obtained spectra of white dwarf spectroscopic standard stars, matched in air mass and observation time to our Seyfert galaxy exposures, to use as atmospheric templates. Experimentation showed that scaling the equivalent width of the atmospheric bands, by adding a constant value to the template and renormalizing, improved the results in some cases, helping to recover good line profiles for the reddest Ca II triplet line. In the case of 3C 390.3, the atmospheric absorption correction was quite critical, since all of the Ca II triplet lines lie in a region of strong atmospheric absorption. In part because of the broad Ca II triplet features in this object, we were able remove the telluric lines successfully.

Reduced, sky-subtracted nuclear spectra corrected for telluric absorption are shown in Figure 1. The spectra have been normalized to the mean counts in the spectral region near the Ca II triplet lines, whose positions are indicated for each object. It is worth emphasizing that a variety of spectral characteristics are present in these galaxies. The Ca II triplet lines show a range of equivalent widths, presenting a challenge for analysis using the FCQ technique in some cases. Also, a number of nuclear emission features, including broad O I λ8446, [Fe II] λ8616, Paschen, and the Ca II triplet itself in emission, appear in our spectra and must be removed before analysis with FCQ. In fact, for two galaxies, Mrk 335 and Mrk 509, no velocity information
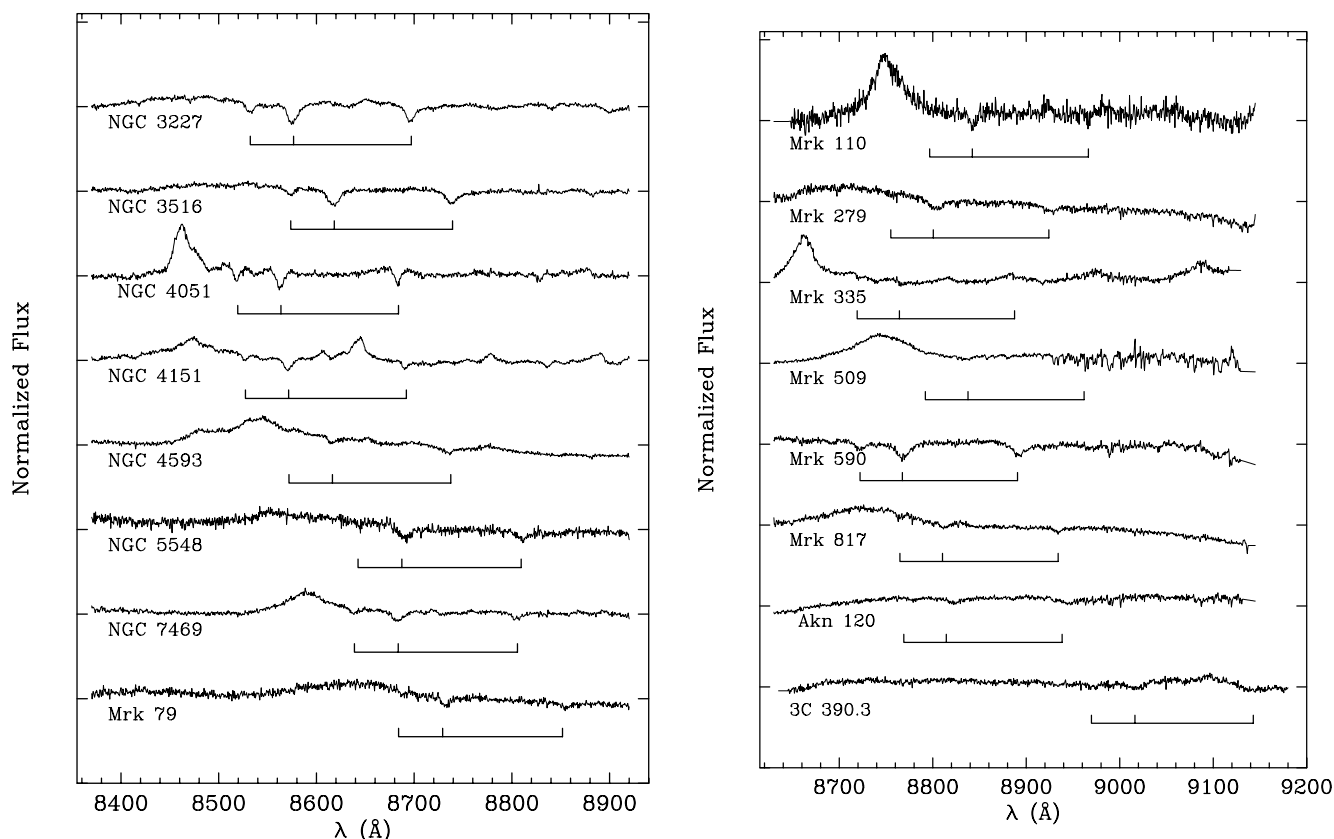
Fig. 1.—Reduced spectra with telluric absorption correction and relative flux calibration applied. The position of the Ca II triplet lines are indicated by the bar with three ticks below each spectrum. The tick marks on the left-hand vertical axis indicate the zero points for each spectrum, giving a sense of the broad range in Ca II triplet equivalent width.

could be obtained (see § 4). Given the association of AGNs and starbursts, we must also keep in mind that the strength of the Ca II triplet lines may be enhanced by young stellar populations rich in late-type supergiant stars (e.g., Terlevich et al. 1990; C. Nelson & M. Whittle 2004, in preparation).

2.2. *Removal of Nuclear Emission*

Even in the far-red, the strength of the nuclear emission from type 1 AGNs relative to the contribution from the host galaxy makes obtaining high signal-to-noise ratio spectra of the stellar absorption features a difficult task: effectively, the nuclear continuum is a source of noise. Also, broad- and narrow-line nuclear emission, even when not affecting the Ca II triplet lines, must be carefully removed before the velocity dispersion measurements can be made. In some cases, in which the stellar absorption lines are strong and the nuclear emission is weak, it was possible to include the nucleus of the galaxy in our long-slit extractions without further processing. For other galaxies, however, the central rows of the long-slit spectra had to be corrected for contaminating emission features or, when the absorption features were entirely lost in the noise, excluded altogether. O I $\lambda8446$ and [Fe II] $\lambda8616$ could often be removed by the subtraction of a single or double Gaussian fit. In other galaxies the blending of emission lines and continuum was more complex, producing an irregular continuum shape near the Ca II triplet lines. In several cases, this required subtraction of a model of the unresolved nuclear spectrum prior to the dispersion measurements.

To produce the model, a narrow spectrum, usually two or three pixels wide centered on the nucleus, was extracted. Next,

the weak Ca II triplet absorption features were removed from the model by subtracting the spectrum of a stellar template, which was broadened and scaled until the absorption lines vanished. Then, using spectra of nearby ninth- or tenth-magnitude SAO stars obtained prior to each galaxy exposure, we produced a seeing profile along the slit. This was combined with the model nuclear spectrum and subtracted from the original long-slit data to correct for the contamination by the nuclear emission. The most important effect of this procedure is that it removes the irregular continuum shape from spectra immediately adjacent to the nucleus. This was particularly helpful in NGC 4051, NGC 4151, and NGC 4593, where the continuum on the blue side of the spectrum is distinctly uneven (compare Figs. 1 and 2). This allowed us to extract spectra for the velocity dispersion analysis much closer to the nucleus than would have been possible otherwise, resulting in a higher signal-to-noise ratio and ensuring that as much of the bulge light was included as possible.

2.3. *Velocity Dispersion Measurements*

Velocity dispersions were obtained by analysis of the bulge line-of-sight velocity distribution (LOSVD) using the FCQ method (Bender 1990). For each galaxy a spectral region, including only the Ca II triplet lines and a small section of continuum on either side, was used in the analysis (rest wavelength 8460–8716 Å). In most cases, the width of the spectrum along the slit was chosen to cover at least 1 kpc across each galaxy. For a few nearby galaxies, we found that extending the slit all the way out to r_e (see Table 2) actually degraded the signal-to-noise ratio while yielding effectively the same dispersion. In
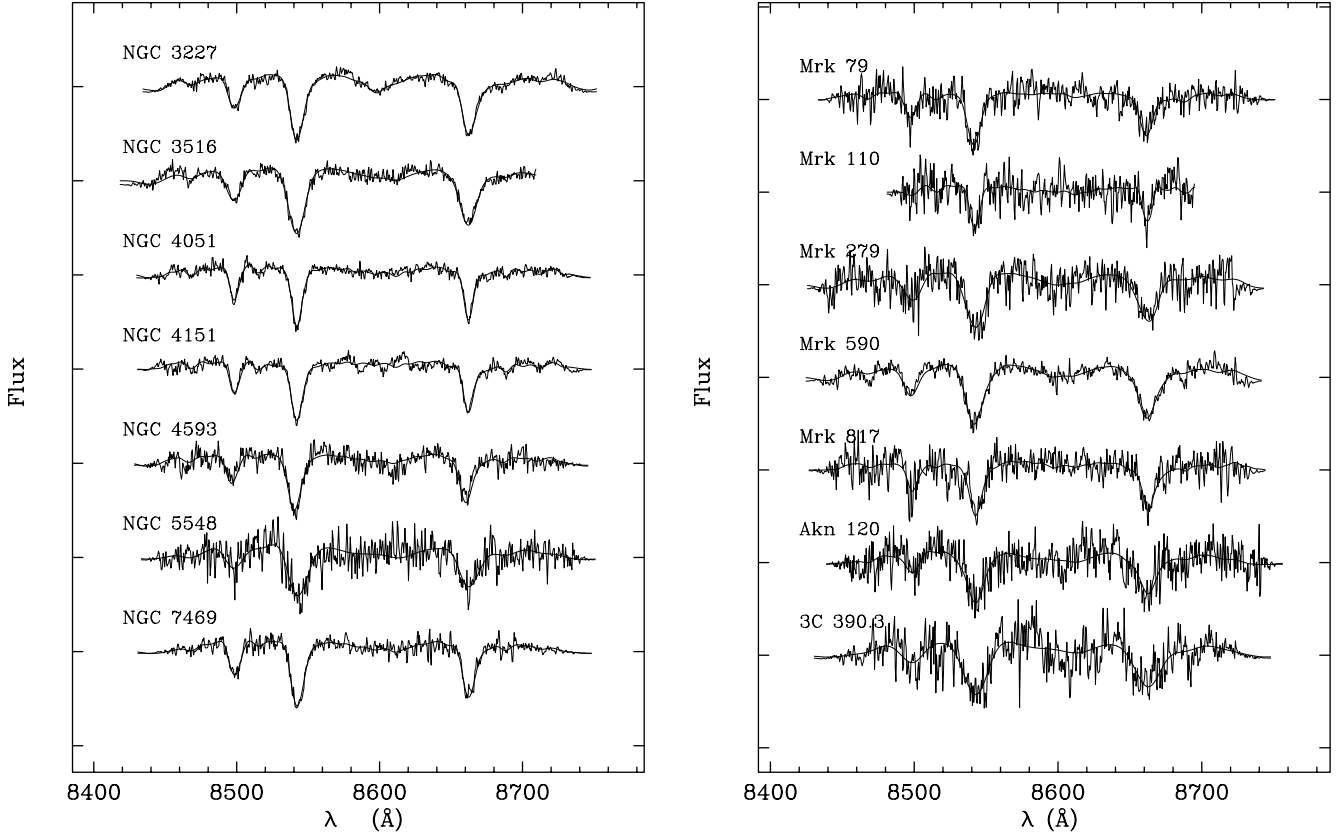
Fig. 2.—Finished spectra that were input to FCQ and also the broadened stellar template. The spectra have been scaled so that the middle line in the Ca II triplet has approximately the same depth in each galaxy.

these cases we opted for the shorter slit length. For the fainter targets an optimal extraction-maximizing signal-to-noise ratio was used. Although this does not generally correspond to r_e as used by Gebhardt et al. (2000a) in defining the M_{BH}-σ_e relation, given the difficulties posed by the nuclear emission it was a reasonable and unavoidable compromise. Nevertheless, our spectra include bulge starlight far enough from the nucleus to be beyond the influence of the black hole, while excluding emission from the kinematically colder galaxy disk.

Gauss-Hermite polynomials were fitted to the LOSVD to determine the bulge systemic velocity, V_*, and the bulge stellar velocity dispersion, σ_*. The uncertainties in V_* and σ_* were estimated by running the FCQ algorithm on Monte Carlo simulations of the data, created using a stellar template convolved with the LOSVD and adding in noise to match that of the observed spectrum. The results for the sample are given in Table 1, including M_{BH} values. Figure 2 shows the data used in the FCQ analysis shifted to the rest frame along with the template broadened by the derived LOSVD.

Velocity dispersions for six of our sample galaxies were published by Ferrarese et al. (2001). A comparison of our results with theirs is shown in Figure 3. We find that our values agree with theirs quite closely, with a marginal tendency for our dispersions to be larger at the low-σ_* end. This may be a consequence of our narrower slit (they used $2''$), which excludes more disk light: a result that may be important for systems with smaller bulges.

3. BULGE MAGNITUDES

To investigate the reported deviations of AGNs from the M_{BH}-M_{bul} relation discussed in § 1, we have used archival *HST*

images to measure bulge magnitudes. Ten of the Seyfert 1 galaxies in our sample were observed in the program of WFPC2 snapshots (Malkan et al. 1998) using the F606W filter and another, NGC 4151, was observed with the F547M filter. The main difficulty in determining the bulge magnitudes from these images was removing the point-source nucleus, which is unfortunately saturated in the F606W images. To accomplish

TABLE 1
Velocity Dispersions in Seyfert 1 Galaxies

Name	Aperture (arcsec)	$\sigma_* \pm \epsilon$ (km s^{-1})	$cz \pm \epsilon$ (km s^{-1})	log M_{BH}[a] ($M_\odot$)
NGC 3227............	4.7	136 ± 4	1187 ± 5	$7.56^{+0.14}_{-0.21}$
NGC 3516............	4.3	181 ± 5	2657 ± 6	$7.23^{+0.08}_{-0.09}$
NGC 4051............	5.6	89 ± 3	743 ± 6	$6.15^{+0.32}_{-0.45}$
NGC 4151............	6.5	97 ± 3	1020 ± 6	$7.08^{+0.23}_{-0.38}$
NGC 4593............	6.5	135 ± 6	2602 ± 7	$6.82^{+0.25}_{-0.67}$
NGC 5548............	2.2	201 ± 12	5100 ± 15	$7.97^{+0.07}_{-0.07}$
NGC 7469............	4.7	131 ± 5	4947 ± 7	$6.88^{+0.30}_{-6.88}$
Mrk 79.................	4.1	130 ± 12	6540 ± 8	$8.01^{+0.14}_{-0.35}$
Mrk 110...............	4.7	91 ± 25	10509 ± 13	$6.89^{+0.13}_{-0.21}$
Mrk 279...............	4.7	197 ± 12	9062 ± 12	$7.41^{+0.10}_{-0.10}$
Mrk 335...............	...	...	...	$6.58^{+0.14}_{-0.13}$
Mrk 509...............	...	...	...	$7.96^{+0.05}_{-0.06}$
Mrk 590...............	4.7	189 ± 6	7904 ± 7	$7.14^{+0.10}_{-0.09}$
Mrk 817...............	4.7	120 ± 15	9409 ± 11	$7.55^{+0.11}_{-0.12}$
Ark 120................	3.0	221 ± 17	9575 ± 15	$8.27^{+0.08}_{-0.12}$
3C 390.3..............	3.6	273 ± 16	16640 ± 15	$8.57^{+0.12}_{-0.21}$

[a] The black hole masses are those obtained using the rms BLR widths. Sources are Onken et al. (2003) for NGC 3227, NGC 3516, and NGC 4593; Ho (1999) for NGC 7469; and Kaspi et al. (2000) for the rest.
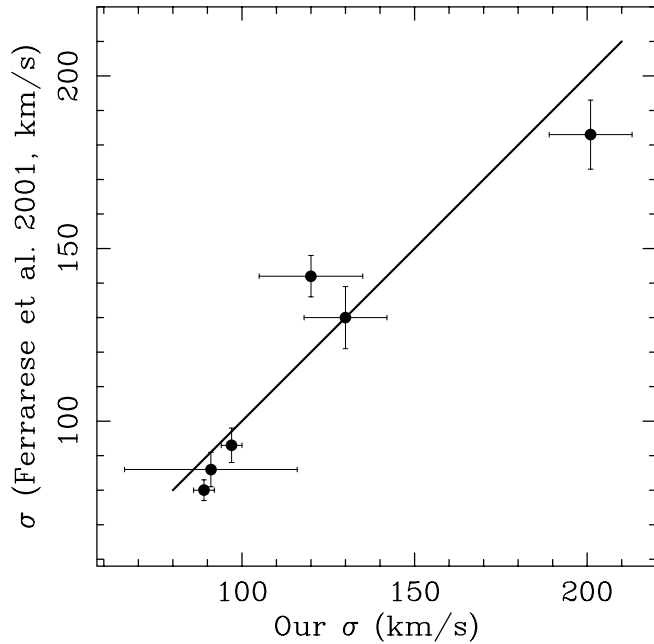
Fig. 3.—Measurements of σ_* compared with those of Ferrarese et al. (2001). The solid line is $X = Y$.

this, model point-spread functions (PSFs), created using the Tiny Tim software package (Krist 1995), were shifted, scaled, and subtracted from the images. The scale factor that produced a minimum rms deviation in the residual image in an annulus incorporating the innermost unsaturated pixels was chosen as an initial guess. Since this tends to overestimate the nuclear luminosity, further trial-and-error scaling of the PSF around

this value allowed us to fine-tune the results; the final best subtraction was judged by examining the removal of peculiar features of the outer PSF (rays and ringlike structures) in the residual images. Typically, we found that a range of scale factors produced acceptable results. The resulting uncertainty in the bulge magnitudes, which given the subjective nature of the PSF scaling we uniformly take to be ±0.2 mag, was folded into our error estimates. Because the galaxy bulges are reasonably large in the images ($r_e \sim 50$–100 pixels in most cases), our results do not depend critically on PSF subtraction. The purpose is mainly to remove the extended wings of the unresolved nuclear emission and recover as much of the inner bulge light as possible. For most objects, we were able to extend our bulge profile analysis down to about $0\overset{''}{.}5$.

Other complications included removing the cosmic ray hits from the images and accounting for emission lines from the narrow-line region (NLR). About 90% of the cosmic rays were removed automatically using a script written in IRAF. Of the remaining cosmic rays, those close to the nucleus were removed by hand. The broad bandpass of the F606W filter includes the [O III] $\lambda5007$, [N II] $\lambda\lambda6548$, 6584, and Hα emission lines that arise in the NLR and will not be removed with the pointlike nucleus. Using the STSDAS task *calcphot* and the model Seyfert 2 galaxy spectrum provided by the SYNPHOT package, we were able to estimate the NLR flux by scaling the model spectrum to match the [O III] flux tabulated in Whittle (1992a). The [O III] fluxes are almost all rated quality "a" by Whittle, indicating that they were obtained through large apertures and that there is good agreement when more than one measurement has been published. Thus, we are confident that we have accounted for the bulk of the NLR emission. This provided a correction to our bulge magnitude estimates and is listed in Table 2.

TABLE 2
Bulge Magnitudes in Seyfert 1 Galaxies

Name[a]	μ_e or μ_0[b] (F606W) (mag)	r_e or r_0[c] (arcsec)	$m_{\rm bul}$ (F606W) (mag)	$\Delta m_{\rm NLR}$ (F606W) (mag)	$M_{\rm bul}$ (F606W) (mag)
NGC 3227	18.31 ± 0.16	2.63 ± 0.26	13.24 ± 0.36	0.09	-18.19 ± 0.49
NGC 3516	19.43 ± 0.12	7.41 ± 0.55	11.91 ± 0.29	0.02	-21.19 ± 0.44
NGC 4051	18.58 ± 0.12	3.10 ± 0.23	13.08 ± 0.30	0.05	-18.53 ± 0.44
NGC 4151	21.40 ± 0.09	20.86 ± 1.59	11.52 ± 0.28	0.00	-20.20 ± 0.43
NGC 4593	20.63 ± 0.17	12.44 ± 1.30	12.01 ± 0.37	0.01	-20.87 ± 0.46
NGC 5548	21.49 ± 0.26	11.03 ± 3.20	12.89 ± 0.71	0.06	-21.31 ± 0.78
NGC 7469	19.66 ± 0.14	5.21 ± 0.44	12.93 ± 0.32	0.06	-21.15 ± 0.45
Mrk 79	21.41 ± 0.28	5.68 ± 0.70	14.46 ± 0.45	0.16	-20.29 ± 0.56
Mrk 279	20.31 ± 0.15	3.89 ± 0.41	14.53 ± 0.39	0.06	-20.86 ± 0.51
Mrk 590*	15.99 ± 0.03	0.71 ± 0.02	14.79 ± 0.21	0.03	-20.25 ± 0.39
Mrk 817*	18.25 ± 0.09	0.98 ± 0.13	16.54 ± 0.39	0.44	-18.58 ± 0.51

[a] An asterisk indicates that an exponential bulge was fitted to the data; all others are $r^{1/4}$-law fits.
[b] μ_e and μ_0 are the surface brightness fitting parameters for $r^{1/4}$-law and exponential forms of the luminosity profile, respectively.
[c] r_e and r_0 are the scale length fitting parameters for $r^{1/4}$-law and exponential forms of the luminosity profile, respectively.

Ideally, two-dimensional direct fitting techniques, such as that of Peng et al. (2002), and a less restricted model, e.g., a Sersic function, could and should be used to investigate the bulge morphologies of these galaxies. We note in the descriptions of the individual galaxies below (§ 4) that the bulge profiles of Mrk 590 and Mrk 817 are better fitted by exponentials than $r^{1/4}$ laws. Also, some display inner spirals, dust lanes, lenses, and bars that further complicate the analysis. However, accounting for these difficulties and the uncertainties associated with NLR emission and saturated PSFs is outside the scope of our program. Thus, in this paper we adopt either the $r^{1/4}$-law or exponential fits to the azimuthally averaged luminosity profiles and use these to estimate bulge magnitude.

We used the IRAF task *ellipse* to produce luminosity profiles from the image isophotes that were then fitted with the sum of an exponential or $r^{1/4}$-law bulge and an exponential disk. In carrying out the fits, it is important to avoid getting trapped in spurious minima of χ^2. The procedure we adopted to ensure meaningful results was to fit the disk region first. Then, holding the disk parameters fixed, we included a fit to the bulge. As a final step, we fitted both bulge and disk simultaneously, allowing all parameters to vary, using the parameter values from the previous steps as the initial guess. The luminosity profiles and fits are plotted in Figure 4. Note the presence of bars or inner ovals in a few galaxies (e.g., NGC 4593, Mrk 79, and NGC 7469), seen as a run of excess light over the fit, between the bulge and disk. We generally excluded these regions from the analysis. Bulge magnitudes were then estimated from the scale length and surface brightness parameters of the fits, assuming $H_0 = 75$ km s^{-1} Mpc^{-1} (as used by Kaspi et al. 2000) to calculate black hole mass. Foreground extinction from the Milky Way has been removed, but no correction for dust within the host galaxy has been applied. The results are given in Table 2 and notes on the characteristics of individual galaxies are given in § 4.

We estimated the error in the bulge magnitudes using Monte Carlo simulations. Random noise with the same rms deviation as the fit to the luminosity profiles was added to the data and the profile was refitted. The resulting standard deviations in the fit parameters after 30 trials was then propagated through to estimate the error in bulge magnitudes from the fitting. These were then added in quadrature to the uncertainty in the nuclear magnitudes and adopted as the uncertainties listed in Table 2. We also include an uncertainty of 15% in the distances of each galaxy to compute the final errors in the absolute magnitudes.

Bulge magnitudes for several of the same Seyfert galaxies were tabulated by McLure & Dunlop (2001), some measured using the same *HST* images, while others were taken from the photographic study of Baggett et al. (1998). In Figure 5, we plot our values against the McLure & Dunlop (2001) results, where we have corrected their values to our choice of H_0 and to the F606W bandpass (since they quote $M_{\rm bul}$ in the R bandpass). The solid line shows $X = Y$, and suggests no systematic trends, although the large scatter (rms = 1.3 mag, compared with the combined error estimate of 1.0 mag) does indicate some disagreement in a number of galaxies. Although McLure & Dunlop (2001) were careful to avoid saturating the nucleus in their own observations of quasar hosts, they do not discuss how they handled the saturated nuclei in the (Malkan et al. 1998) snapshots. Also, in Mrk 817 we have a rather large correction for NLR emission, which to our knowledge was not considered by McLure & Dunlop (2001). In any case the large scatter, while disappointing, is not far outside what might be expected from the uncertainties in the measurements.

4. NOTES ON INDIVIDUAL SEYFERT 1 GALAXIES

NGC 3227.—The active continuum is weak, and the Ca II triplet lines are seen at nearly full strength (C. Nelson & M. Whittle 2004, in preparation). Note the presence of Paschen absorption lines in Figure 2 (particularly Pa14 $\lambda8598.4$, between the two stronger Ca II triplet lines), indicating the presence of a young stellar population. An F5 III star was used as a velocity template in this case. The bulge of this galaxy is surprisingly small and faint given its Hubble type (SABa; de Vaucouleurs et al. 1991) and σ_*, perhaps as a result of the dusty nuclear regions (Malkan et al. 1998).

NGC 4051.—Weak Ca II triplet in emission can be seen in this object as well as strong and relatively narrow O I $\lambda8446$ and [Fe II] $\lambda8618$ emission. All of these were removed by combining model nuclear emission with a seeing star as described in § 2.2.

NGC 4151.—Nuclear emission features in the Ca II triplet spectrum were removed by combining model nuclear emission with a seeing star. Long and short exposure images for this object were obtained with the F547M filter. This allowed an accurate subtraction of the nucleus. Also, this filter excludes most of the optical emission lines, so no correction was applied for the NLR. The magnitude in Table 2 has been converted to the F606W bandpass using *calcphot*, assuming the spectrum is well represented by the Sb template in the SYNPHOT package. This is the most discrepant point in Figure 5, for which McLure & Dunlop (2001) used the bulge-disk decomposition of Baggett et al. (1998) based on ground-based photographic imaging.

NGC 4593.—Nuclear emission features were removed by combining model nuclear emission with a seeing star.

NGC 5548.—Since the velocity dispersion falls off quite rapidly with distance from the nucleus, a narrow spectral extraction was used.

NGC 7469.—The position angle and long-slit extraction were chosen to avoid knots in the well-known starburst ring (Wilson et al. 1991). O I $\lambda8446$ was removed with a Gaussian fit.

Mrk 110.—This was the poorest spectrum in our sample and as a consequence we quote a large error estimate for the velocity dispersion. O I $\lambda8446$ removed with a Gaussian fit.

Mrk 279.—Broad, weak O I $\lambda8446$ was removed in normal continuum subtraction.

Mrk 335.—Ca II triplet in emission (Malkan & Filippenko 1983) could not be removed.

Mrk 509.—No Ca II triplet features were detected owing to the strong nuclear continuum.

Mrk 590.—The bulge of this galaxy is better fit by an exponential than an $r^{1/4}$ law.

Mrk 817.—O I $\lambda8446$ was removed with a double Gaussian fit. The bulge is better fitted by an exponential than an $r^{1/4}$ law.

3C 390.3.—Because of its high redshift, the Ca II triplet lines fall in a region relatively free of night sky emission lines, eliminating the need for nod-and-shuffle sky subtraction. However, the atmospheric absorption is severe; careful division by atmospheric template was remarkably successful.

5. THE $M_{\rm BH}$-σ_* RELATION FOR ACTIVE GALAXIES

In Figure 6 we plot as filled circles our σ_* values versus $M_{\rm BH}$ values from reverberation mapping. We use the $M_{\rm BH}$ values directly from the literature, but note that these are calculated assuming random orbits for BLR clouds following equation (5) in Kaspi et al. (2000; see also Wandel et al. 1999). We discuss the significance of this assumption in § 6. Furthermore, as
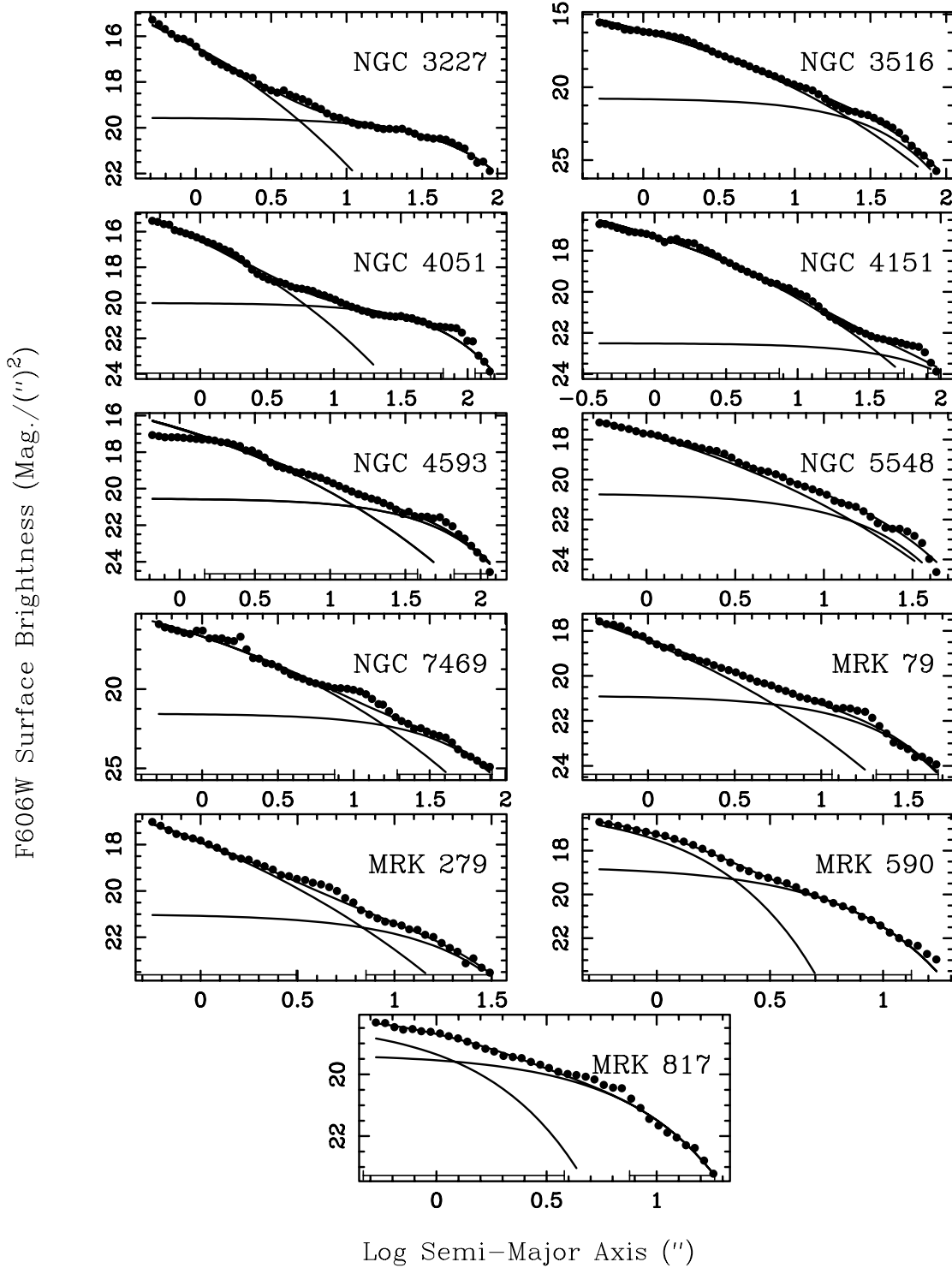
FIG. 4.—Luminosity profiles and bulge-disk decomposition for Seyfert 1 galaxies from *HST* images. The emission from the nucleus has already been subtracted from the profiles. Note the exponential bulges in Mrk 590 and Mrk 817. A horizontal line shows regions included in the fitting (if not present, all of the data was used); gaps are usually associated with bars.

mentioned in the note to Table 1, the black hole masses are those calculated using the rms Hβ FWHM rather than the mean values, i.e., the variable component of the line (see Wandel et al. 1999). Having tried both, we find no significant differences in our results using one or the other. For comparison, we also plot as crosses elliptical and S0 galaxies from Gebhardt et al. (2000a), where $M_{\rm BH}$ has been determined from stellar dynamical orbit-based modeling. The solid line is the derivation of the $M_{\rm BH}$-σ_e relation from Tremaine et al. (2002) and the dashed line

is a fit to the Seyfert galaxies using the ordinary least-squares bisector method (OLSB; Isobe et al. 1990). The 14 Seyfert galaxies, by themselves, show a strong correlation (linear correlation coefficient $R = 0.73$ for the rms masses with probability of no correlation $P_{\rm null} = 0.29\%$ and slightly better for the mean masses $R = 0.80$ and $P_{\rm null} = 0.065\%$).

In Figure 6 there appears to be no significant evidence for an offset for Seyfert galaxies from the Tremaine et al. (2002) relation. Computing the residuals of the AGNs to the solid line,
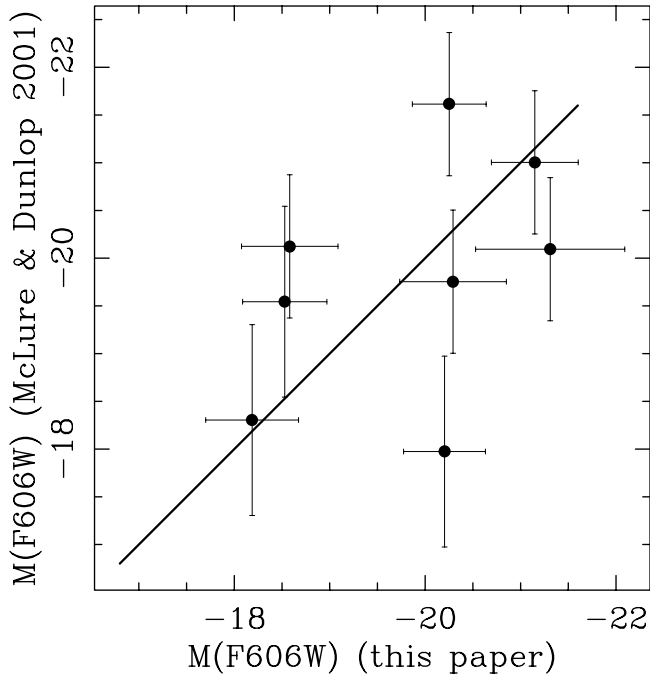
FIG. 5.—Measurements of M_{bul} compared with those of McLure & Dunlop (2001) rescaled to $H_0 = 75$ km s^{-1} Mpc^{-1}. The solid line is $X = Y$.
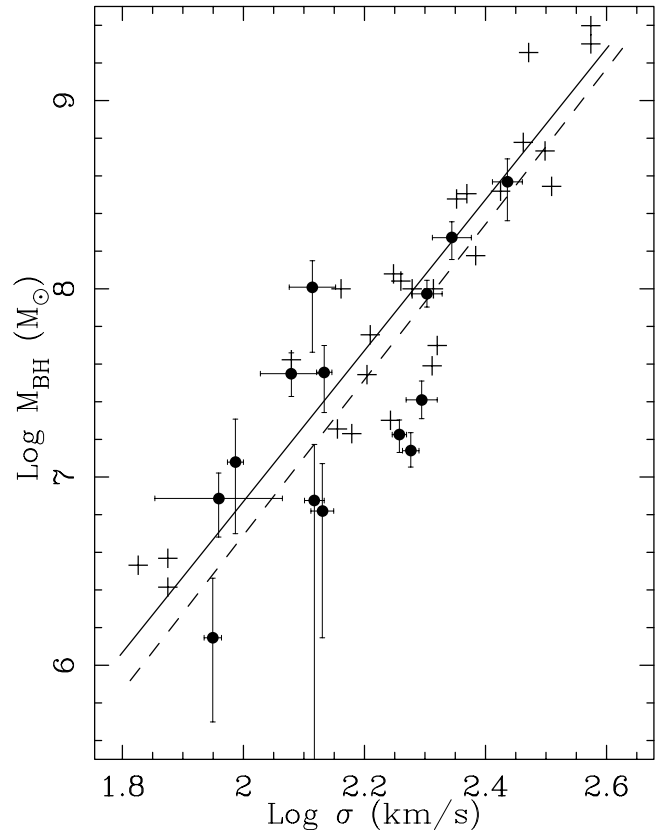

FIG. 6.—Black hole mass plotted against velocity dispersion for Seyfert galaxies from Table 1, shown as filled circles, and for normal elliptical and S0 galaxies from Gebhardt et al. (2000a), shown as crosses. The black hole masses for Seyfert galaxies are determined from reverberation mapping, while the Gebhardt et al. (2000a) masses are from dynamical modeling of the nuclear stellar kinematics. The solid line is the relation calculated by Tremaine et al. (2002) and the dashed line is a fit to the Seyfert galaxies using the ordinary least-squares bisector method (Isobe et al. 1990).

we find an average shift of $\Delta \log M_{BH} = 0.21$ in the direction of lower black hole masses at a given σ_*, with a standard deviation of 0.46 dex for the 14 AGNs. Clearly, the significance of such a shift is marginal and distinctly not in agreement with the factor of 5 found by Ho (1999) using the M_{BH}-M_{bul} relation.

The exact value of the slope of M_{BH}-σ_* has been a matter of some debate. The slope 4.1 ± 0.5 for the AGN sample is not significantly different from the slope for the normal galaxies, although given the uncertainty it is beyond the ability of this data set to provide a decisive result. A larger sample of AGNs might well provide interesting constraints.

These results effectively confirm the conclusions of Gebhardt et al. (2000b), Nelson (2000), and Ferrarese et al. (2001) that there is no distinct difference in the M_{BH}-σ_e relation between active and nonactive galaxies. Furthermore, it suggests that the reverberation mapping technique for determining black hole masses in AGNs produces results that are consistent with masses determined by stellar dynamical and gasdynamical techniques. We should emphasize, however, that this is an indirect check on reverberation mapping. A direct verification may be possible should a target of reverberation mapping campaigns go into a low-luminosity phase, allowing the application of standard stellar dynamical analysis. Indeed, an *HST* cycle 12 proposal involving target of opportunity observations of NGC 3227 and NGC 4151 has been approved (Prop. No. 9849, PI: B. Peterson).

Our results, of course, are very encouraging for investigations of the role of black hole mass in AGNs. However, the sample used here is by necessity composed of lower luminosity Seyfert 1 galaxies. Further study of the M_{BH}-σ_e relation is needed to validate its application to more luminous AGN.

6. THE M_{BH}-M_{bul} RELATION FOR AGNs REVISITED AND THE FABER-JACKSON RELATION

It is essentially conventional wisdom that active nuclei are preferentially found in bulge-dominated galaxies (e.g., Ho

et al. 1997). Confirmation of the M_{BH}-σ_* relation for Seyfert galaxies provides important support for this tenet of AGN physics. It strongly reinforces the notion that the bulge gravitational potential plays an important role in determining the properties of activity in galaxies. However, if we accept that the M_{BH}-σ_* relation is the same for Seyfert galaxies as it is for normal bulges and ellipticals, what do we make of previous claims of smaller M_{BH} values in AGNs for a given bulge luminosity, discussed in the introduction to this paper?

In Figure 7, we plot M_{bul} for the Seyfert 1 galaxies in Table 2 versus the reverberation mapping M_{BH} values. Again for comparison, ellipticals and bulges from the Gebhardt et al. (2000a) sample are plotted as crosses, where we have converted their absolute V magnitudes as published in Faber et al. (1997) to the F606W bandpass and scaled to $H_0 = 75$ km s^{-1} Mpc^{-1}. Given the narrow range of colors for the Gebhardt et al. (2000a) sample ($\langle B - V \rangle = 0.95$ mag, $\sigma = 0.047$ mag) and the expectation that the Seyfert bulge colors are likely to be more scattered, we choose to apply the correction to the ellipticals. The conversion was determined using the template elliptical galaxy from the SYNPHOT package and the *calcphot* task ($M_{F606W} = V - 0.33$ mag).

Although not a strong trend, the majority of Seyfert galaxies lie below and to the right of the OLSB fit to the ellipticals, shown as the solid line. This is consistent with the report by Ho (1999) of lower black hole masses at a given bulge magnitude. The median deviation in black hole mass for the Seyfert
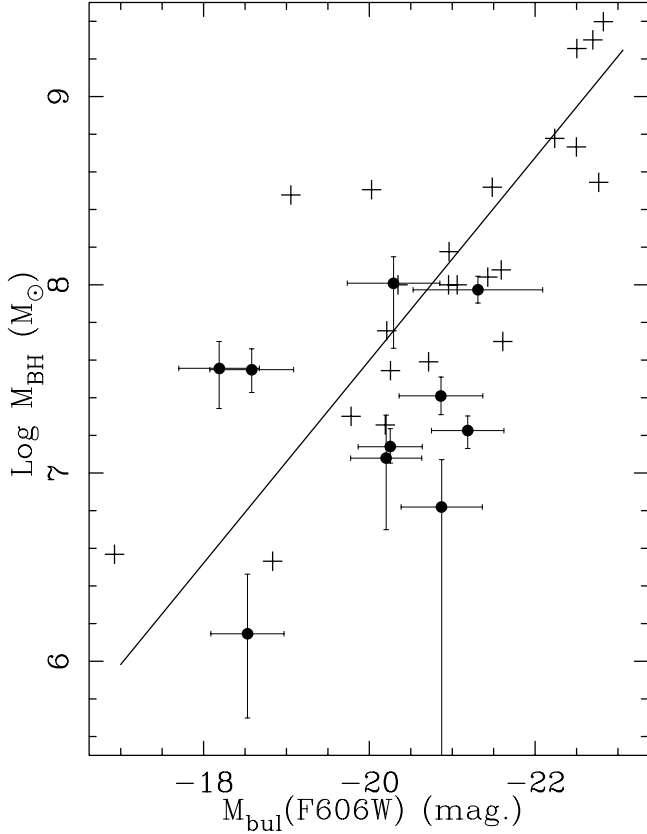
FIG. 7.—Black hole mass plotted against bulge absolute magnitude for Seyfert galaxies (*filled circles*) and the Gebhardt et al. (2000a) sample (*crosses*), rescaled to $H_0 = 75$ km s^{-1} Mpc^{-1}. The solid line is a fit to the elliptical galaxies.

FIG. 8.—Faber-Jackson plot for Seyfert 1 galaxies from Table 2 (*filled circles*) and for elliptical and S0 galaxies from Gebhardt et al. (2000a; *crosses*). The solid line is a fit to the elliptical sample and the dashed line is a fit to the Seyfert galaxies. The Seyfert galaxies in the sample show a tendency for brighter $M_{\rm bul}$ at a given σ_*.

galaxies from the fit to the normal galaxies is 0.4 dex, or about a factor of 2.5. There is really no significant correlation for the Seyfert galaxies, (linear correlation coefficient $R = -0.16$), compared with a strong trend found for the ellipticals ($R = -0.80$). This may be due in part to the smaller sample size, but this cannot be the whole story, since the Seyfert galaxies show a strong correlation between $M_{\rm BH}$ and σ_* (see § 5).

We suggest that it is the bulge luminosities, not the black hole masses, which are the origin of the deviation. Taken in this way, the bulges of Seyfert galaxies are on average 0.7 mag brighter than normal ellipticals with similar black hole masses based on the distribution of points in Figure 7. Strong support for this interpretation is found by plotting the Faber-Jackson diagram, σ_* versus $M_{\rm bul}$, for both samples, shown in Figure 8. We find that at a given σ_*, the Seyfert galaxies tend to lie above the fit to the normal galaxies. The mean residual in $M_{\rm bul}$ for the Seyfert galaxies relative to the normal galaxy fit is -0.4 mag. Furthermore, there is a moderately strong correlation for the Seyfert galaxies, ($R = -0.6$). This improvement over the results for $M_{\rm bul}$ versus $M_{\rm BH}$ naturally suggests that $M_{\rm bul}$ is more closely related to σ_* than to $M_{\rm BH}$, and that the increase in bulge luminosities with black hole masses is secondary and follows through their mutual trends with velocity dispersion.

The result is identical to that of Nelson & Whittle (1996), who found a similar offset for a much larger sample, consisting of mostly Seyfert 2 galaxies. The result also confirms the earlier conclusions of Whittle (1992b, 1992c), who used galaxy rotation amplitude and FWHM$_{\rm [O\,III]}$ as virial parameters to demonstrate a tendency for brighter bulges in Seyfert galaxies than normal galaxies of the same bulge mass. Some ambiguity
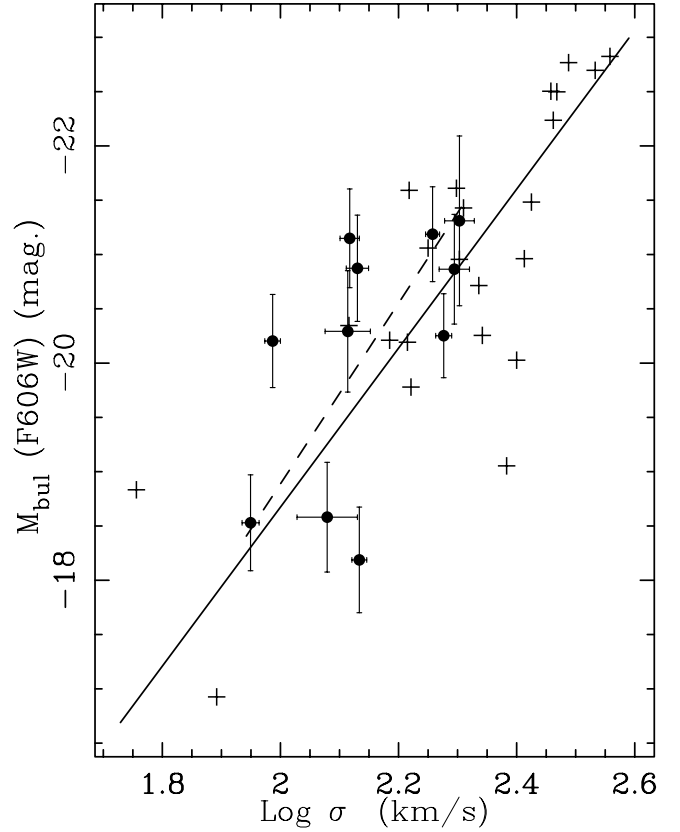
remained, however, since the bulge magnitudes in those studies were not obtained by bulge/disk decomposition. Instead, after correcting for nuclear emission, the relation between bulge-to-disk ratio and Hubble stage of Simien & de Vaucouleurs (1986) was used to estimate bulge magnitudes. This technique has been criticized by McLure & Dunlop (2001) and Wandel (2002), who suggest that it results in overestimates of $M_{\rm bul}$. The present confirmation of the offset in the Faber-Jackson relation for Seyfert galaxies using explicit bulge-disk-nucleus separation, however, suggests that while there is admittedly significant scatter, any systematic errors are small.

In contrast to the Ho (1999) result, McLure & Dunlop (2001) and Wandel (2002) claim no deviation in the $M_{\rm BH}$-$M_{\rm bul}$ relation for Seyfert and normal galaxies. We can reconcile this conflict by recognizing that McLure & Dunlop (2001) choose to calculate $M_{\rm BH}$ assuming a disklike morphology and purely rotational kinematics for the BLR as opposed to the random orbits assumed by Kaspi et al. (2000). Thus, the observed line widths depend on the orbital velocity, V, and the inclination of the BLR disk. After making assumptions about the range and mean of the distribution of inclinations, they adopt a relation between orbital velocity and the BLR line widths, $V = 1.5 \times$ FWHM, distinctly different from the case for random cloud orbits, $V = \sqrt{3}/2 \times$ FWHM. This results in $M_{\rm BH}$ values that are a factor of 3 *larger* than the standard reverberation mapping calculations in which the BLR velocity field is assumed to be random. Therefore, if we were to couple their bulge measurements with the $M_{\rm BH}$ values calculated assuming random BLR motions, we should also get brighter bulges at a

given $M_{\rm BH}$ for AGNs. Of course, the specific form of the BLR velocity field is unknown. Our results, at least for the case of random cloud motions, are consistent with an identical $M_{\rm BH}$-σ_e relation for Seyfert and normal galaxies and a tendency for brighter bulges in Seyfert galaxies.

A different argument applies to the Wandel (2002) analysis, which assumes that random motions dominate in the BLR. This study reports a correlation between Hβ line width and the suspected overestimate of $M_{\rm bul}$ resulting from the application of the Simien & de Vaucouleurs (1986) B/T morphology relation discussed above. This correlation is then used to correct the $M_{\rm bul}$ values, resulting in a reduction of the bulge luminosities for much of the sample. However, the physical link between BLR kinematics and differences in B/T is not established. It is therefore unclear why such a correction should be required. Removing this correction from Wandel's results should also result in relatively brighter bulges for AGNs.

The most straightforward interpretation of these results is that Seyfert galaxies have, on average, brighter bulges as a result of lower M/L ratios. Thus, the difference is one of stellar population, indicating that Seyfert galaxies are more likely than nonactive galaxies to have had recent episodes of nuclear star formation. This is certainly plausible, given the voluminous research on the link between AGNs and starburst galaxies. It is informative to use model stellar populations to estimate the age and mass fraction of the bulge required to produce a brightening of this degree. Guy Worthey's Dial-a-Galaxy Website (Worthey 1994) allows users to mix stellar population models of different ages, metallicities, etc., to estimate the changes to the integrated light properties of galaxy spectra. A simple run, with two solar metallicity populations of 1 and 12 Gyr, shows that if 15% of the total mass is from the young population the R-band magnitude will be ~0.5 mag brighter than a population composed completely of old stars. Obviously, more complex and realistic models could produce similar results. Nevertheless, this simple estimate indicates a typical size and age for a burst of star formation to produce the shift seen in the Seyfert sample.

It is interesting to note that a number of recent morphological studies of Seyfert galaxies have found no evidence for morphological triggers of nuclear starbursts, e.g., galaxy interactions and bars, including subkiloparsec scale bars (e.g., Ho et al. 1997; Pogge & Martini 2002; Regan & Mulchaey 1999). Although it is conceivable that there is a time delay between a galaxy interaction and the onset of nuclear fueling, the result is troubling, since we might expect at least some evidence of the disturbance to remain. A possible solution was hinted at in Nelson & Whittle (1996), based on the fact that Seyfert galaxies are not found outside the general envelope of scatter for normal galaxies in the Faber-Jackson plot. Considering the residuals to the Faber-Jackson relation, they found that the distribution of $\Delta \log \sigma_*$ is considerably narrower, yet overlaps that for nonactive galaxies, a detail that is reproduced in Figure 8. Assuming that the spheroids of normal galaxies exhibit a broad range of star formation histories, perhaps Seyfert galaxies are more akin to normal spirals with above average central star formation rates than to massive starbursts initiated by strong interactions or bars.

7. SUMMARY

We have obtained new measurements of the bulge stellar velocity dispersion in Seyfert 1 galaxies with nuclear black hole masses determined using the reverberation mapping technique. Our results have shown that Seyfert galaxies follow the same correlation between $M_{\rm BH}$ and σ_* as for nonactive galaxies and that reverberation mapping yields black hole masses that are consistent with masses determined through stellar dynamical modeling techniques. We also investigated the origin of previous assertions that the masses of black holes in active galaxies were smaller than those in normal galaxies (or at least underestimated) at a given bulge luminosity. We find that the best explanation is that the bulges are brighter on average in Seyfert galaxies, suggesting lower M/L ratios, most likely as a result of higher star formation rates in their recent history.

REFERENCES

Baggett, W. E., Baggett, S. M., & Anderson, K. S. J. 1998, AJ, 116, 1626
Bender, R. 1990, A&A, 229, 441
Blandford, R. D., & McKee, C. F. 1982, ApJ, 255, 419
Bower, G. A., et al. 1998, ApJ, 492, L111
de Vaucouleurs, G., de Vaucouleurs, A., Corwin, H. G., Jr., Buta, R. J., Paturel, G., & Fouqué, P. 1991, Third Reference Catalogue of Bright Galaxies (New York: Springer)
Dey, A., et al. 2001, NOAO Newsl., 65, 37
Faber, S. M., et al. 1997, AJ, 114, 1771
Ferrarese, L., & Merritt, D. 2000, ApJ, 539, L9
Ferrarese, L., Pogge, R. W., Peterson, B. M., Merritt, D., Wandel, A., & Joseph, C. L. 2001, ApJ, 555, L79
Gebhardt, K., et al. 2000a, ApJ, 539, L13
———. 2000b, ApJ, 543, L5
———. 2003, ApJ, 583, 92
Glazebrook, K., & Bland-Hawthorn, J. 2001, PASP, 113, 197
Ho, L. C. 1999, in Observational Evidence for Black Holes in the Universe, ed. S. K. Chakrabarti (Dordrecht: Kluwer), 153
Ho, L., Filippenko, A. V., & Sargent, W. L. W. 1997, ApJ, 487, 568
Isobe, T., Feigelson, E. D., Akritas, M. G., & Babu, G. J. 1990, ApJ, 364, 104
Kaspi, S., Smith, P. S., Netzer, H., Maoz, D., Januzzi, B. T., & Giveon, U. 2000, ApJ, 533, 631
Kormendy, J. 1993, in The Nearest Active Galaxies, ed. J. Beckman, L. Colina, & H. Netzer (Madrid: Consejo Superior de Investigaciones Científicas), 197
Kormendy, J., & Richstone, D. 1995, ARA&A, 33, 581

Krist, J. 1995, in ASP Conf. Ser. 77, Astronomical Data Analysis Software and Systems IV, ed. R. A. Shaw, H. E. Payne, & J. J. E. Hayes (San Fransisco: ASP), 349
Malkan, M. A., & Filippenko, A. V. 1983, ApJ, 275, 477
Malkan, M. A., Gorjian, V., & Tam, R. 1998, ApJS, 117, 25
McLure, R. J., & Dunlop, J. S. 2001, MNRAS, 327, 199
Nelson, C. H. 2000, ApJ, 544, L91
Nelson, C., & Whittle, M. 1996, ApJ, 465, 96
Netzer, H., & Peterson, B. M. 1997, in Astronomical Time Series, ed. D. Maoz, A. Sternberg, & E. M. Leibowitz (Dordrecht: Kluwer), 85
Onken, C. A., Peterson, B. M., Dietrich, M., Robinson, A., & Salamanca, I. M. 2003, ApJ, 585, 121
Peng, C., Ho, L. C., Impey, C. D., & Rix, H. 2002, AJ, 124, 266
Pogge, R., & Martini, P. 2002, ApJ, 569, 624
Regan, M. W., & Mulchaey, J. S. 1999, AJ, 117, 2676
Simien, F., & de Vaucouleurs, G. 1986, ApJ, 302, 564
Terlevich, E., Diaz, A. I., & Terlevich, R. 1990, MNRAS, 242, 271
Tremaine, S., et al. 2002, ApJ, 574, 740
Wandel, A. 1999, ApJ, 519, L39
———. 2002, ApJ, 565, 762
Wandel, A., Peterson, B. M., & Malkan, M. A. 1999, ApJ, 526, 579
Whittle, M. 1992a, ApJS, 79, 49
———. 1992b, ApJ, 387, 109
———. 1992c, ApJ, 387, 121
Wilson, A. S., Helfer, T. T., Haniff, C. A., & Ward, M. J. 1991, ApJ, 381, 79
Worthey, G. 1994, ApJS, 95, 107